Hindawi
Journal of Nanomaterials
Volume 2021, Article ID 8275987, 11 pages
https://doi.org/10.1155/2021/8275987

Research Article

N-Doped Carbon Dots Derived from Melamine and Triethanolamine for Selective Sensing of Fe^{3+} Ions

Sathishkumar Munusamy,[1] **Sathish Sawminathan**,[2] **Thanigaivelan Arumugham**,[3] **Maura Casales Díaz**,[4] **Srinivas Godavarthi**,[5] **and Mohan Kumar Kesarla**[4]

[1]*Institute of Chemical Biology and Nanomedicine, State Key Laboratory of Chemo/Bio-Sensing and Chemometrics, College of Chemistry and Chemical Engineering, Hunan University, Changsha 410082, China*
[2]*Department of Chemistry, School of Advanced Sciences and Vellore Institute of Technology, Vellore 632014, India*
[3]*Department of Chemical Engineering, Khalifa University, 127788 Abu Dhabi, UAE*
[4]*Instituto de Ciencias Físicas, Universidad Nacional Autónoma de México, Avenida Universidad s/n, 62210 Cuernavaca, MOR, Mexico*
[5]*CONACYT–Universidad Juárez Autónoma de Tabasco, Centro de Investigación de Ciencia y Tecnología Aplicada de Tabasco (CICTAT), Cunduacán, C.P. 86690, Mexico*

Correspondence should be addressed to Mohan Kumar Kesarla; mohan@icf.unam.mx

Received 1 June 2021; Revised 22 July 2021; Accepted 15 September 2021; Published 4 October 2021

Academic Editor: Ester Vazquez

This work reports nitrogen-doped carbon dots (NCDs) as a selective sensing probe to detect Fe^{3+} in water samples. NCD probes were synthesized via solvothermal method using nitrogen-rich melamine and triethanolamine as precursors. Properties of the resulting NCDs were studied using different characterization techniques, through which N-doping was confirmed. The quantum yield of obtained NCDs was measured to be 21%. When excited at 370 nm, the excellent blue emission property makes this probe adoptable for selectively sensing Fe^{3+} in practical water samples. The limit of detection (LOD) was identified as 216 nM with a good linear range between the concentrations of 0.2-2 μM. The obtained LOD is far less than the World Health Organization (WHO) permissible limits of Fe^{3+} in water. Interference studies reveal that the presence of other competing ions did not alter the sensing of Fe^{3+}, even at the presence of 10 equivalents which indicates the high selectivity of NCDs towards Fe^{3+}. The reversibility studies showed that adding a cheap and readily available EDTA ligand to the NCD results in fluorescence regeneration, leading to exceptional reusability for the detection of Fe^{3+}. So, the synthesized NCDs can be used as a suitable probe for the selective determination of Fe^{3+} in real water samples.

1. Introduction

Among nanocarbon materials, carbon dots (CDs) have been given much attention due to their properties such as low cytotoxicity, robust chemical inertness, and good biocompatibility, which are particularly useful in several areas like sensing, imaging, photodegradation, and theranostic applications [1–6]. On the other hand, modification of electronic structures of CDs by doping heteroatoms such as nitrogen is further beneficial, especially in sensing due to enhanced fluorescence quantum yields [6–17]. Hence, extensive research efforts have been dedicated to their synthesis [18–20]. But, to incorporate a heteroatom in carbon framework requires complicated strategies such as high-temperature carbonization of nitrogen compounds, treatment of carbon materials with ammonia at high temperatures, liquid phase polymerization of nitrogen-containing compounds, and chemical vapor deposition with nitrogen-containing compounds as nitrogen sources. But all the techniques mentioned above have drawbacks such as severe synthetic conditions, high cost, complex, and time-consuming processes [21–23]. Even though many other methods are available to synthesize nitrogen-doped carbon dots (NCDs) [24–26], for example, using biomass via green synthesis methods, -broad PL

emission profiles and high quantum yields remained as challenges in the production of CDs. So, the development of inexpensive and scalable synthesis for the production of NCDs remains a requirement.

Metals play an essential part in the physiological functions of biological systems. Among the different metal ions, iron ions play a crucial role in biochemical reactions, oxygen loading, cellular proliferation, enzyme catalysis, etc. However, a lower or higher concentration of Fe^{3+} may lead to severe health concerns such as anemia, organ dysfunction, and skin diseases [27–30]. Considering the extensive use of iron in the day-to-day life of humans, estimating its quantities in water is vital. In detecting metal ions, fluorescence methods have benefits such as high sensitivity, reusability, onsite usage, and relatively economical, over traditional spectrophotometric approaches, which generally require complex sample preparation procedures and expensive instrumentation [31, 32]. Even though several fluorescent sensors have been reported in the literature [33–37], only very few highly selective and susceptible detection of Fe^{3+} ions with reusability exists [36, 37].

The present study described novel fluorescent NCDs that can detect Fe^{3+} ions. For the first time, water-soluble NCDs were made from readily accessible nitrogen-rich precursors like melamine and triethanolamine together, utilizing a cost-effective and straightforward one-pot solvothermal approach without the need for passivation chemicals. Synthesized NCDs were characterized structurally and optically using TEM, XRD, FT-IR, absorption, and fluorescence spectroscopy. These NCDs were shown to have a high sensitivity and selectivity for Fe^{3+} ions in an aqueous solution with a low detection limit. Moreover, other competing metal ions do not affect the optical property of NCDs. Additionally, the real-time application of Fe^{3+} detection was demonstrated by the quantification of Fe^{3+} in water samples.

2. Experimental

2.1. Materials. Melamine (99%), triethanolamine (99.5%), chloroform, methanol, ethanol, and EDTA were purchased from Sigma Aldrich and used without further purification. Likewise, all the metal salts used for sensing applications were purchased from Sigma Aldrich and utilized as such.

2.2. Synthesis of NCDs. NCDs were synthesized using melamine and triethanolamine together as precursors for carbon and nitrogen. Briefly, 500 mg of melamine was dispersed in 20 mL of ethanol using an ultrasonic bath, and 1 mL of triethanolamine was introduced into the above mixture and stirred for half an hour on a magnetic stirrer. Then, this solution mixture was transferred into Teflon lined autoclave and heated at 160°C for four hours. After four hours, the solution was allowed to cool to room temperature naturally. The crude product was purified by silica gel column chromatography with chloroform and methanol as the eluent (70 : 30), collecting the yellow-green fraction. Finally, the portion was concentrated to get the black solid (~11 mg). The obtained NCDs were redispersed in double distilled water as per the requirement.

2.3. Characterization. The UV-vis spectrum of the purified NCDs and different cations was monitored from 200 to 800 nm using Shimadzu 3300 UV-double beam spectrophotometer. FT-IR spectra of the obtained NCDs were recorded using the Thermo Scientific Nicolet iS10 ATR-FTIR instrument to get surface functionalization information before and after sensing of Fe^{3+}. The size, shape, and SAED patterns of NCDs were obtained using an FEI Technai G2-20 twin high-resolution transmission electron microscope (HRTEM) with an operating acceleration voltage of 200 kV. The sample for HRTEM was prepared by dispersing and sonicating the NCDs in methanol and then dropping them on a Cu grid coated with holey carbon film and allowed to dry. XRD pattern was collected using Bruker D8 Advanced eco with Cu Kα = 1.54 Å in the 2θ range of 10 to 90°. Prior to recording the XRD patterns, the instrument was calibrated with Lanthanum hexaboride (LaB_6). Finally, all the PL measurements including sensing of Fe^{3+} were carried out using a Hitachi F-2000 spectrophotometer.

2.4. Quantum Yield Measurements. Quantum yield (QY) was determined using the below equation

$$\Phi S = \Phi R \frac{A_R(\lambda_R) n_s^2 I_s}{A_S(\lambda_S) n_R^2 I_R}, \quad (1)$$

where ΦS and ΦR are quantum yields of sample and reference, respectively; $A_R(\lambda_R)$ and $A_s(\lambda_s)$ are the absorbance of the reference and sample at excitation wavelengths; n_S and n_R are refractive indices of the sample medium and reference medium, respectively; I_S and I_R are the integrated fluorescence intensities of sample and reference, respectively. Because of the stable luminescent properties of quinine sulfate (Φ = 54% at 340 nm), this was used as a reference in 0.1 M H_2SO_4 to determine the QY of NCDs [22].

2.5. Detection of Metal Ions Using NCDs. To detect metal ions using NCDs, precursors like $Cu(NO_3)_2$, KBr, $NaNO_2$, $MgSO_4$, $MnSO_4$, H_2O, $NiCl_2.6H_2O$, $PbSO_4$, SeS_2, $Sr(NO_3)_2$, $ZnSO_4$. $7H_2O$, $CaSO_4$, $2H_2O$, $BaCl_2$, $HgCl_2$, $FeCl_2.4H_20$, BiOCl, and $FeCl_3$ were used. The ion solution with a concentration of 100 μM was added into 2 mL of predispersed NCDs solution and recorded the PL spectra immediately. All the PL spectra were recorded at an excitation wavelength of 370 nm.

3. Results and Discussion

The solvothermal method was adopted to synthesize NCDs where melamine and triethanolamine together act as carbon and nitrogen sources. Upon solvothermal treatment at 160°C for four hours, the solution turned yellow and emitted greenish-blue when kept under UV light (Scheme 1).

After purification of NCDs by column chromatography using the eluent mixture of chloroform and methanol

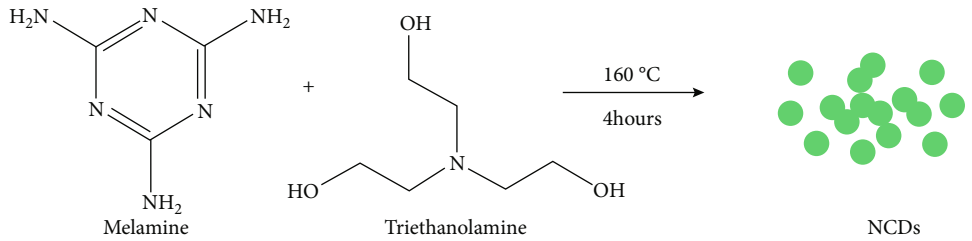

Scheme 1: Synthesis of NCDs by solvothermal methods.

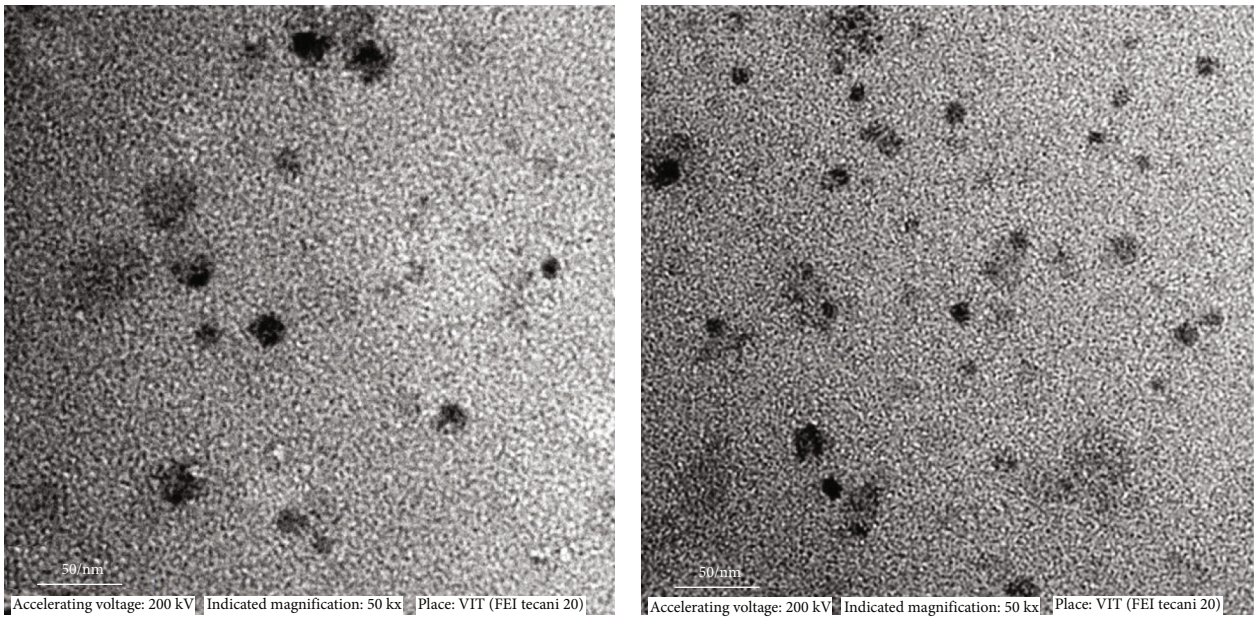

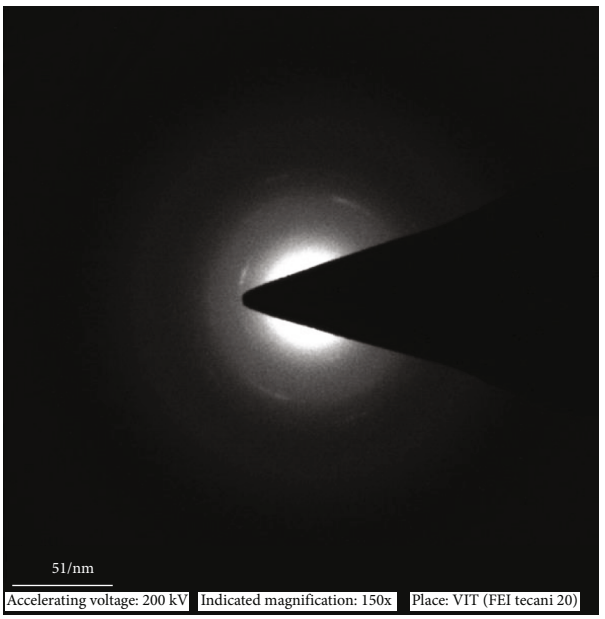

Figure 1: (a) and (b) HRTEM images of synthesized NCDs with scale bar 50 nm and (c) SAED pattern of the obtained NCDs.

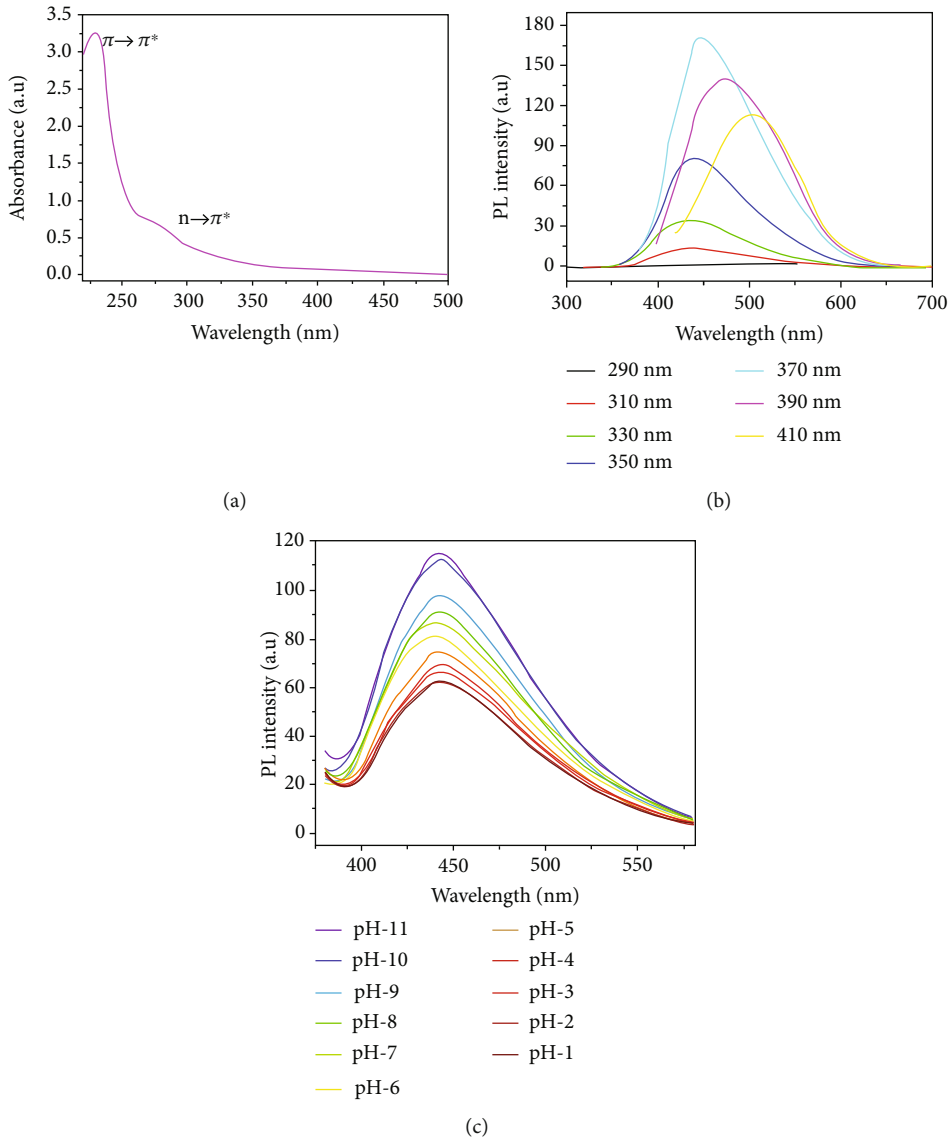

Figure 2: (a) UV-vis spectra of purified NCDs in methanol solution. (b) PL spectra of NCDs under various excitation wavelengths. (c) The effect of pH on fluorescence intensity of NCDs. All the experiments were carried out in a water medium.

(70 : 30), the as-prepared sample showed the relative fluorescence quantum yield of 21% using quinine sulfate reference. The observed high quantum yield was ascribed to nitrogen doping in the carbon framework [19].

Figure S1 of supplementary information shows the X-ray diffraction pattern of the as-obtained NCDs. From the XRD pattern, it is clear that a broad peak is centered at $2\theta = 26.87^{\circ}$, which corresponds to (002), due to the highly disordered graphitic structure associated with NCDs. The weak diffraction peak around 43° is due to the presence of highly disordered amorphous carbon with a fractional extent of graphitization [38]. In general, graphitic carbon appears at 26.5°, and the slight shift in diffraction angle is due to the doping of nitrogen into carbon, which resembles more or less like amorphous carbon nitride [39]. So indirectly, N-doping was confirmed with XRD results.

FT-IR spectra were used to identify the surface functionalization. Figure S2 of supplementary information depicts

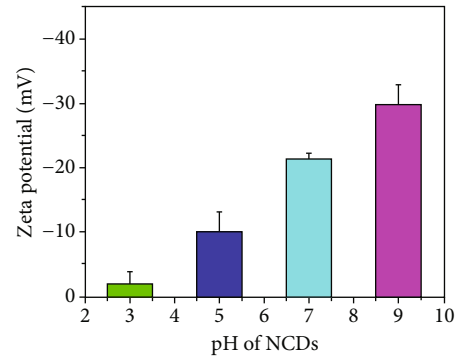

Figure 3: Zeta potential as a function of pH for NCDs.

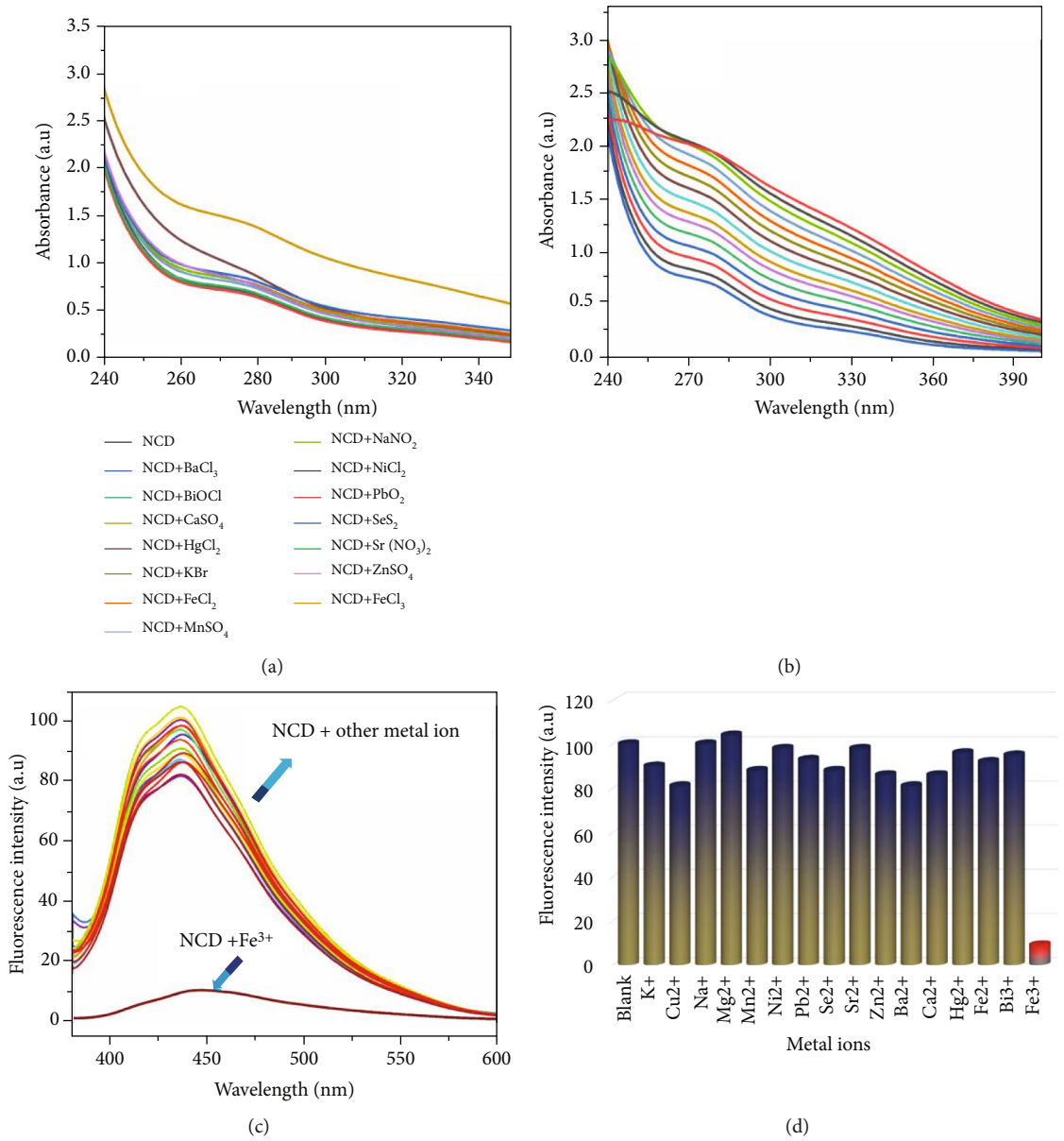

Figure 4: (a) UV-vis spectra of NCDs in the presence of different metal ions. (b) UV-vis spectra of NCDs with the gradual increase in the concentration of Fe^{3+}. (c) PL spectra of NCDs in the presence of various metal ions. (d) Bar diagrams showing selectivity of NCDs towards Fe^{3+} sensing. All the experiments were carried out in a water medium.

FT-IR of the synthesized NCDs. FT-IR shows a broad absorption band at 3323 cm^{-1} which indicates the presence of -OH/-NH_2 groups. The bands around 2830 and 2943 cm^{-1} were due to the -C-H stretching, and the strong band at 1022 cm^{-1} reveals the presence of -C-O stretching vibrations. The peak at 1675 cm^{-1} indicates the stretching of -C=N/-C=O and -C-H deformation appears around 1450 cm^{-1}. The presence of nitrogen in the NCDs was evident from FT-IR, and the surface was functionalized with -OH and -NH_2 groups.

High-resolution transmission electron microscopy of the as-synthesized NCDs were shown in Figures 1(a) and 1(b), and the selected area diffraction patterns (SAED) was shown in Figure 1(c). It is clear from the HRTEM that the NCDs were well dispersed, and the size of the dots was in the range of 5 to 20 nm. The selected area diffraction pattern also reveals the semicrystalline nature of the formed NCDs due to disordered graphitic structure associated with NCDs (Figure 1(c)).

The optical properties of the NCDs were studied using a UV-vis spectrophotometer in double-distilled water (Figure 2(a)). It is very clear from UV-vis spectra, the band around 230 nm appeared due to $\pi \longrightarrow \pi *$ transition of aromatic conjugated sp^2 domains, the shoulder peak at around 275 nm corresponds to the $n \longrightarrow \pi *$ transition of carbonyl groups, and the broad peak centered at approximately 330 nm indicates the surface state defects induced by nitrogen doping [40]. PL spectra of as-synthesized NCDs at various excitation wavelengths are shown in Figure 2(b) at different excitation wavelengths. The synthesized NCDs

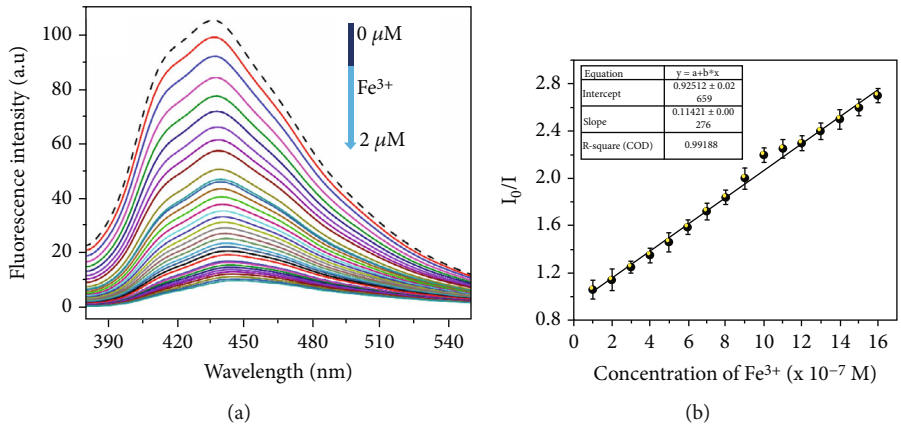

FIGURE 5: (a) PL spectra of NCDs with increasing concentration of Fe^{3+} and (b) S-V plot of quenching of NCDs with Fe^{3+}.

exhibit excitation-dependent fluorescence upon increasing the excitation wavelength from 290 to 410 nm; the PL emission peak shifts gradually from 425 nm to 525 nm. The fluorescence intensity under 370 nm excitation shows a maximum emission peak at 435 nm among the various excitation wavelengths. In addition, an apparent redshift was observed with a remarkable decrease in PL intensity when the excitation wavelength was increased beyond 370 nm. The excitation-dependent PL spectra were attributed to the presence of functionalities like (C = O/N, -NH_2), which leads to $\pi * \longrightarrow n$ transitions of surface states. These phenomena occur due to doping of nitrogen hetero atom, leading to defective surface states with a concomitant effect on PL enhancement.

The effect of pH on the fluorescence emission intensity of NCDs solution was also evaluated in the range of 1 to 11 (Figure 2(c)). The pH of the NCDs solution was adjusted to the desired value by adding either 0.1 M HCl or NaOH. Medium with the pH range of 1-4 has shown a significant reduction in the PL. Whereas neutral or basic pH has caused a dramatic increase in the PL intensity. This behavior can be attributed to the different degrees of protonation at lower pH solutions. At lower pH solutions, the primary sites at the surface of NCDs tend to neutralize, generating a lower net surface charge which provides the NCDs with hydrophobic and aggregative properties with subsequent aggregation caused quenching (ACQ) of PL. The NCDs show good PL behavior in basic environments, and it is found that pH 6 to 11 was the best pH values for the sensing system. To further understand the mechanism of NCDs behavior with different pH, their Zeta potentials were determined in acidic, neutral, and alkaline conditions. As shown in Figure 3, in the neutral or basic pH condition, the NCDs showed overall negative surface potential due to free -OH and -NH_2 functional groups, which ensures high colloidal stability due to electrostatic repulsion between NCDs. As the pH of the solution decreases from 9 to 3, the negative zeta potential tends to decrease, which is in accordance with our assumption. The decrease in negative zeta potential is due to the protonation of the surface functional groups. As the pH medium of NCDs after the purification is ~7, there is no need to adjust the pH of the solution before proceeding to metal sensing.

3.1. Selectivity of NCDs towards Fe^{3+} Ions. To figure out which metal ions that NCDs can recognize selectively, NCDs sensing of different metals were monitored by changes in UV-vis and fluorescence spectra in the presence of various metal ions like K^+, Cu^{2+}, Na^+, Mg^{2+}, Mn^{2+}, Ni^{2+}, Pb^{2+}, Se^{2+}, Sr^{2+}, Zn^{2+}, Ca^{2+}, Ba^{2+}, Hg^{2+}, Bi^{3+}, Fe^{2+}, and Fe^{3+} in 100 μM concentration of each element. It is very clear from Figure 4(a); no significant absorbance changes were observed except upon the addition of $FeCl_3$. The intensity of the NCDs absorption peak at around 270 nm showed a substantial increase over the addition of Fe^{3+}, which provided the preliminary insight about pursuing our experiments towards detecting Fe^{3+} selectivity of NCDs towards sensing Fe^{3+} (Figure 4(b)). Moreover, a linear relationship was found between the absorption intensity of NCDs and Fe^{3+} concentration (Figure S3 of supplementary information) between 2 μM and 20 μM concentrations.

The fluorescence response of NCDs with various metal ions (100 μM) was studied at an excitation wavelength of 370 nm. As shown in Figure 4(c), although NCDs exhibit emission at 435 nm, we observed that there are no significant changes in the fluorescence intensities upon introduction of different metal ions like K^+, Cu^{2+}, Na^+, Mg^{2+}, Mn^{2+}, Ni^{2+}, Pb^{2+}, Se^{2+}, Sr^{2+}, Zn^{2+}, Ca^{2+}, Ba^{2+}, Hg^{2+}, Fe^{2+}, and Bi^{3+}. But over the addition of Fe^{3+} ions, it was observed that NCDs suffered a significant quenching in emission. This experiment revealed that the NCDs are very selective towards sensing Fe^{3+} ions. The selective sensing of Fe^{3+} was demonstrated using the bar diagram in Figure 4(d). This observation encouraged us to believe that the NCDs could be used as potential "turn-off" nanosensors for Fe^{3+} in an aqueous medium.

To check the quantitative applicability of NCDs, fluorescence spectrometric titrations were carried out with increasing concentrations of Fe^{3+}. The titration experiment was performed in the medium of pH 7 using phosphate buffer. Figure 5(a) shows the PL behavior of NCDs with an increasing concentration of 0.2 μM Fe^{3+} in every step. Upon increasing the concentration of Fe^{3+}, the emission peak at 435 nm decreases gradually. As the concentration of Fe^{3+} reached 2 μM, NCDs showed very little fluorescence and perturbance. From the Stern-Volmer (S-V) curve, the linear

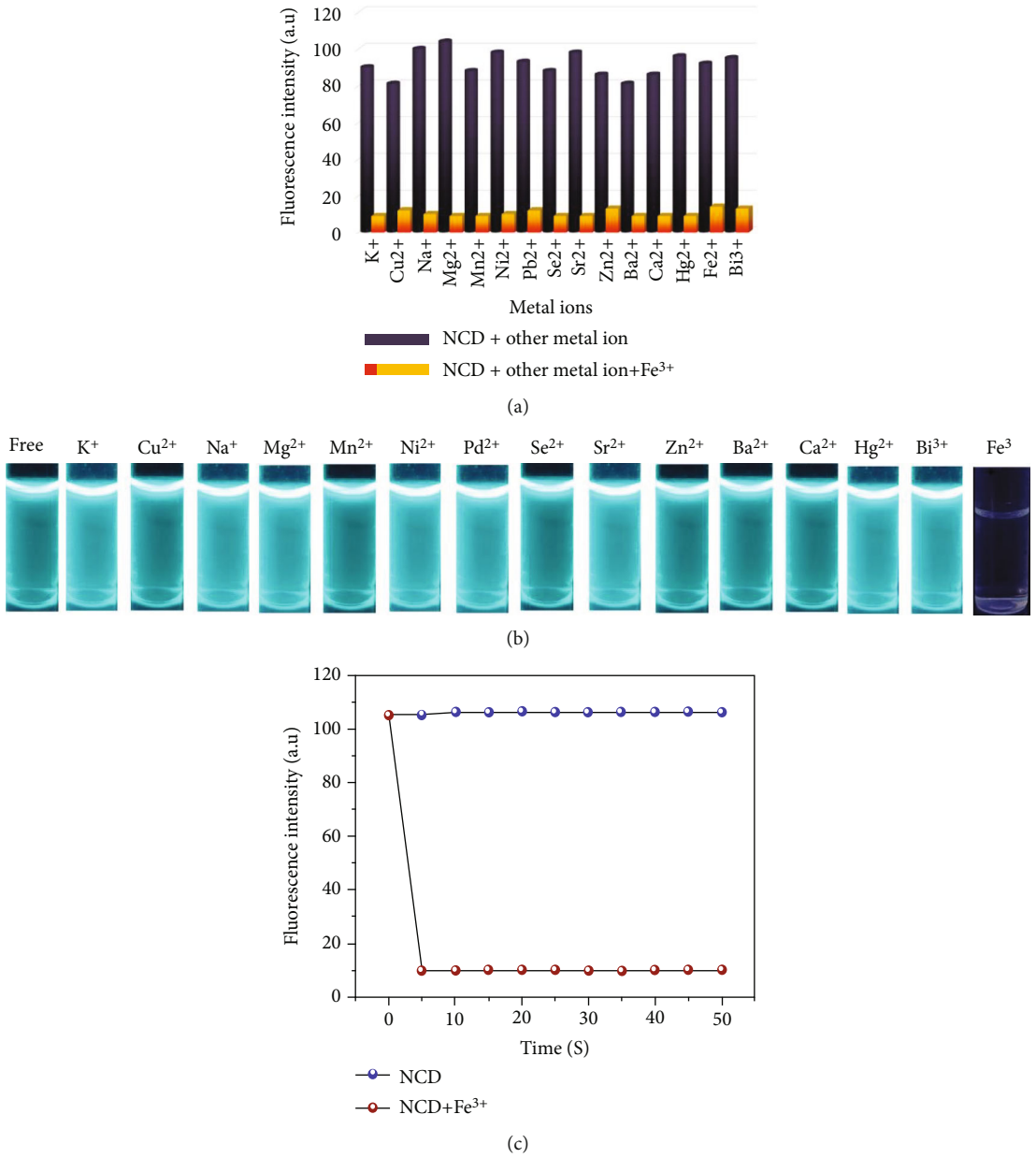

Figure 6: (a) Anti-interference of NCDs in the presence of Fe^{3+} (2 μM) and miscellaneous cations (20 μM) at 435 nm. (b) Fluorescence response time of NCDs over the addition of Fe^{3+}. (c) Photographs of NCDs in the presence of various metals and Fe^{3+} under a UV lamp at 365 nm.

regression was found to be $y = 0.11x + 0.92$. Y and X are Io/I (where Io and I are fluorescence intensity of NCDs without and with Fe^{3+}) and the concentration of Fe^{3+}, respectively. The linear range was displayed for a concentration range of 0.2 to 2 μM with a 0.9925 correlation coefficient (Figure 5(b)). The LOD is determined to be 216 nM/L based on the $3.3\sigma/K$ equation, where σ is the standard deviation and K is the slope of the calibration curve. The obtained LOD is significantly less compared to that of permissible levels of WHO for Fe^{3+} in water (5.36 μmol L^{-1}) [41] and many recent papers (Table S3 of supplementary information). The current observation signifies the use of synthesized NCDs to detect Fe^{3+} with high selectivity and sensitivity.

3.2. Interference and Time Dependence. Interference with the detection of Fe^{3+} with NCDs by other competitive metal ions was investigated. As can be seen from Figure 6(a), the presence of other ions did not disturb the sensing of Fe^{3+}, even at the presence of 10 equivalents, which indicates the high selectivity of NCDs towards Fe^{3+}. Besides, the probe's bright and clear bluish-green emission was completely switched off when viewed under the UV light (Figure 6(b)), whereas other metal ions retained the bluish-green fluorescence. Besides, the fluorescence response time of NCDs to Fe^{3+} was monitored by a time-based fluorescence study. As shown in Figure 6(c), the addition of Fe^{3+} to NCDs caused emissions to quench immediately, and it reached the plateau within 5 seconds. This demonstrates there is an instant

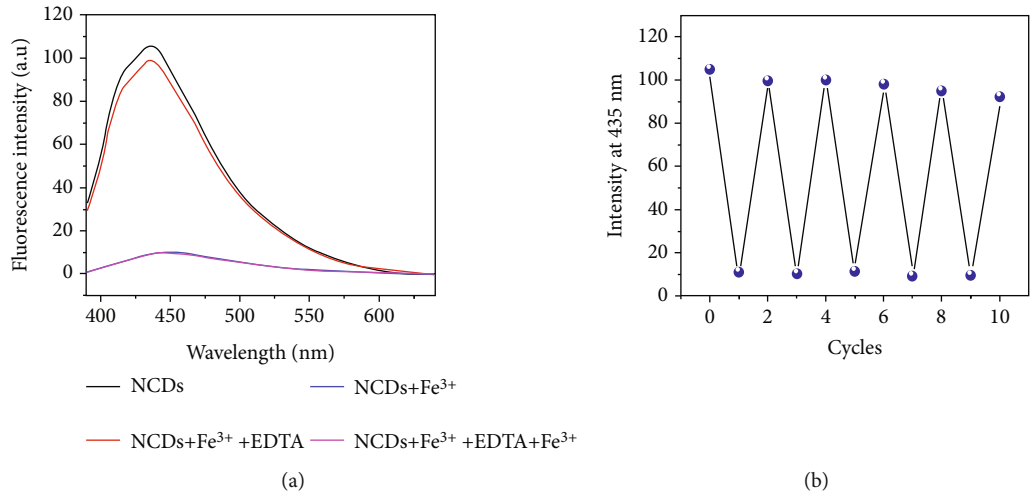

Figure 7: (a) Fluorescence intensity responses of NCD upon addition of Fe^{3+} + EDTA. (b) Number of sequential detections of Fe^{3+} and EDTA.

reaction between NCDs and Fe^{3+}. This indicates that Fe^{3+} can be detected free of culture time with NCDs, which may be used in real-time applications.

3.3. Reversibility Study. Reversibility is the essential parameter of the probe for the real-time application and economic aspect [42]. A fervent complexing agent EDTA has been added to the NCD-Fe^{3+} system to validate NCD sensors' reversibility towards Fe^{3+}. In the beginning, free NCDs show intense fluorescence, and the addition of Fe^{3+} almost completely quenched the emission. Upon the addition of five equivalents of Na_2-EDTA to the above solution, the emission was immediately registered. As shown in Figure 7(a), the addition of EDTA to the NCDs and Fe^{3+} mixture caused nearly immediate recovery of the fluorescence due to the formation of EDTA + Fe^{3+} complex and consequent regeneration of previous intensity of free NCDs. The 'ON-OFF-ON' behavior of the NCDs fluorescence emission at 435nm canbe repeated around five times with a slight decrease in the initial emissionintensity (Figure 7(b)). This experiment suggests that adding a cheap and readily available EDTA ligand to the NCDs results in excellent reusability for the detection of Fe^{3+}.

3.4. Application of NCDs in Practical Water Analysis. To determine the practical utility of NCDs, we performed fluorescence detection of Fe^{3+} using NCDs in water samples collected from various bodies of water throughout the Vellore district, India. First, water samples were spiked with known Fe^{3+} concentrations, and their effect on the fluorescence of NCDs was determined by recording the emission intensity at 435 nm. Then, three consecutive measurements were made to determine the mean Fe^{3+} detection value. As shown in Table 1, a satisfactory recovery and relative standard deviation (R.S.D.) were detected with the spiked Fe^{3+} concentration. These findings suggest that NCDs can detect Fe^{3+} with high selectivity and precise quantification.

Table 1: Estimation of Fe^{3+} ion quantity in collected water samples using NCDs.

Synod	Water samples[a]	Fe^{3+} spiked (μM)	Fe^{3+} found (μM)	Recovery (%)	R.S.D[b] ($n = 3$) (%)
1	Tap water	1×10^{-5}	0.93×10^{-5}	93	.36
2	Lake water	1×10^{-5}	0.95×10^{-5}	95	0.18
3	Well water	1×10^{-5}	0.93×10^{-5}	93	0.21
4	Mineral water	1×10^{-5}	0.96×10^{-5}	96	0.49
5	Distilled water	1×10^{-5}	0.92×10^{-5}	92	0.28
6	Purified water	1×10^{-5}	0.95×10^{-5}	95	0.61

[a]Water samples were collected from throughout the Vellore district, India; [b]relative standard deviation.

3.5. Fluorescence Quenching Mechanism. The fluorescence quenching of NCDs up on the introduction of Fe^{3+} may be explained as follows (Figure 8). When there are no Fe^{3+} ions, upon incidence of the light, NCDs captivate energy, and electrons move from the ground (HOMO) to the excited (LUMO) state. When the electrons fall back to the ground state, radiative recombination of electrons and holes results in fluorescence emission.

As confirmed from FTIR, the surface of NCDs has -NH_2 and -OH groups on their surfaces. The relatively high selectivity of the NCDs towards Fe^{3+} was attributed to the half-filled 3D orbitals, short-range ionic radius, and unique coordinate interaction of Fe^{3+}. Those properties made Fe^{3+} possess greater binding affinity and quicker chelating kinetics for hydroxyl, carboxyl, and amino groups on the surface of N-CDs, which would promote the coordination reaction between N-CDs and Fe^{3+}. Therefore, when Fe^{3+} comes in contact with surface states of NCDs, the five half-filled d

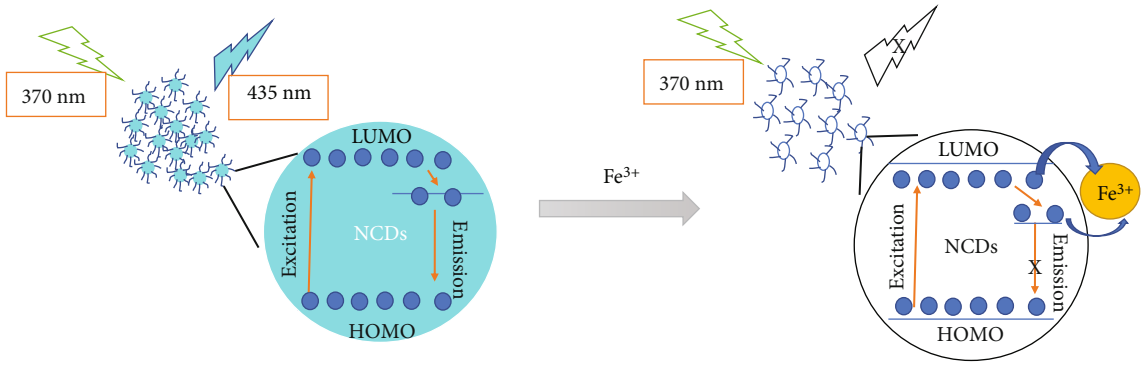

Figure 8: Schematic representation of quenching in emission selectively with Fe^{3+} ions.

orbitals of Fe^{3+} take up the excited electron, forming nonradiative recombination, which simultaneously leads to fluorescence quenching shown in Figure 8. This selective interaction of Fe^{3+} with NCDs was further confirmed by FT-IR analysis (Figure S4 of supplementary information). The NCDs clear vibration peak at 3323 cm^{-1} arising from -OH/NH_2 functional got diminished over the addition of Fe^{3+}. Whereas Cu^{2+} (potential interferant for Fe^{3+}) has significantly less influence on the FT-IR spectra of NCDs (Figure S4).

The S-V plot can also explain the fluorescent quenching mechanism. It denotes the relationship between the fluorescence intensity and the metal ion concentration. In essence, the quenching mechanisms are two types. One is complexation (static quenching), and another one is collisional deactivation (dynamic quenching). The S-V plot can be used to verify the preceding mechanism. The general form of the S-V equation is as follows.

$$\frac{F_0}{F} = 1 + K_{sv}[Q], \tag{2}$$

where F_0 and F are the fluorescence intensity of the NCDs before and after the presence of metal ions. K_{sv} is the S-V constant, and Q is the Quencher concentration. The calibration curve (Figure 5(b)) was obtained from the plot of F_0/F versus the concentration of Fe^{3+}, and it exhibits a linear relationship between x and y-axis over the range of 0-2 μM, which denotes static quenching, resulting in the formation of a nonfluorescent complex formation between Fe^{3+} and NCDs. The plausible explanation for the occurrence of static quenching can be further confirmed by performing the fluorescence sensing experiments at different sets of temperatures, i.e., 25°C, 30°C, and 35°C, maintaining optimal conditions for all other parameters (Figure 9). For each temperature, the S-V calibration curve was drawn. It was noticed that the value of K_{sv} decreased as the temperature increased (as shown in Table 2) because raising temperature tends to reduce the binding interactions result in static quenching. As a result, the findings are consistent with a static quenching process.

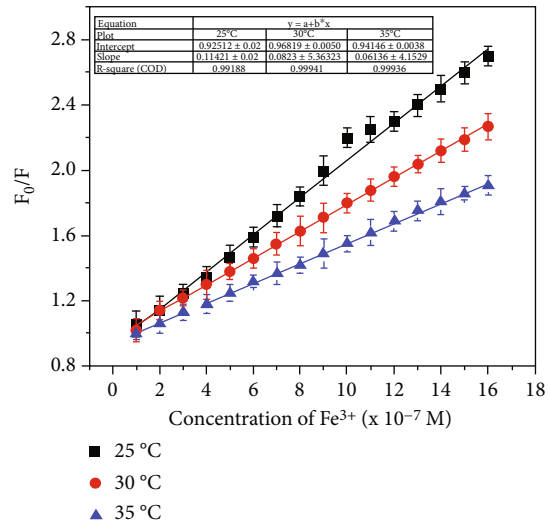

Figure 9: S-V plot for fluorescence quenching of NCDs by Fe^{3+} ions at different temperatures.

Table 2: S-V constant of interaction between NCDs and Fe^{3+} at different temperatures.

S. no	Temperature (°C)	K_{sv} (M^{-1})	R^2
1	25	1.14×10^6	0.9918
2	30	0.82×10^6	0.9994
3	35	0.61×10^6	0.9936

4. Conclusion

Nitrogen-doped carbon dots (NCDs) were synthesized successfully by the solvothermal method using melamine and triethanolamine as carbon/nitrogen precursors with a quantum yield of 21%. Surface functionalization and the presence of nitrogen were confirmed using FTIR. HRTEM results revealed that the NCDs were in the range of 5-15 nm. The excitation-dependent PL nature was observed from PL spectra. PL experiments revealed that the synthesized NCDs show good potential towards sensitive and selective detection of Fe^{3+} with a detection limit of 216 nM/L, far less than WHO permissible limits. Furthermore, a cheap and readily

available ligand can regenerate the emission from the probe leading to its excellent reusability. Applicability in the practical water analysis suggests that NCDs can detect Fe^{3+} with high selectivity and precise quantification.

Data Availability

The data used to support the findings of this study are included within the article and in the supplementary information file.

Conflicts of Interest

The authors declare no conflict of interest.

Acknowledgments

Dr. Kesarla acknowledges the financial support from Programa de Apoyo a Proyectos de Investigación e Innovación Tecnológica (PAPIIT), project no. IA201321. We thank Mr. José Juan Ramos Hernández, Academic Technician, for his continuous support in various characterizations.

Supplementary Materials

Supplementary information file available with Figures S1 to S4 and Tables S1 as referred in the main text. *(Supplementary Materials)*

References

[1] B. B. Chen, M. L. Liu, and C. Z. Huang, "Recent advances of carbon dots in imaging-guided theranostics," *TrAC Trends in Analytical Chemistry*, vol. 134, article 116116, 2021.

[2] P. Jayasekhar Babu, S. Saranya, Y. D. Singh, M. Venkataswamy, A. M. Raichur, and M. Doble, "Photoluminescence carbon nano dots for the conductivity based optical sensing of dopamine and bioimaging applications," *Optical Materials*, vol. 117, article 111120, 2021.

[3] S. Hu, Y. Ding, Q. Chang, J. Yang, and K. Lin, "Chlorine-functionalized carbon dots for highly efficient photodegradation of pollutants under visible-light irradiation," *Applied Surface Science*, vol. 355, pp. 774–777, 2015.

[4] M. Zheng, S. Liu, J. Li et al., "Integrating oxaliplatin with highly luminescent carbon dots: an unprecedented theranostic agent for personalized medicine," *Advanced Materials*, vol. 26, no. 21, pp. 3554–3560, 2014.

[5] X. Tu, Y. Ma, Y. Cao, J. Huang, M. Zhang, and Z. Zhang, "PEGylated carbon nanoparticles for efficient in vitro photothermal cancer therapy," *Journal of Materials Chemistry B*, vol. 2, no. 15, pp. 2184–2192, 2014.

[6] M. Ashrafizadeh, R. Mohammadinejad, S. K. Kailasa, Z. Ahmadi, E. G. Afshar, and A. Pardakhty, "Carbon dots as versatile nanoarchitectures for the treatment of neurological disorders and their theranostic applications: a review," *Advances in Colloid and Interface Science*, vol. 278, article 102123, 2020.

[7] Y. Man, W.-S. Zou, W.-L. Kong et al., "Brightly blue triazine-doped carbon dots for selective determination of Cu(II) in environment and imaging in cell," *Journal of Photochemistry and Photobiology A: Chemistry*, vol. 416, article 113321, 2021.

[8] M. Bonet-San-Emeterio, M. Algarra, M. Petković, and M. del Valle, "Modification of electrodes with N -and S -doped carbon dots. Evaluation of the electrochemical response," *Talanta*, vol. 212, article 120806, 2020.

[9] Z. Zhang and Z. Fan, "Application of cerium-nitrogen co-doped carbon quantum dots to the detection of tetracyclines residues and bioimaging," *Microchemical Journal*, vol. 165, article 106139, 2021.

[10] L. Sun, Y. Liu, Y. Wang et al., "Nitrogen and sulfur co-doped carbon dots as selective and visual sensors for monitoring cobalt ions," *Optical Materials*, vol. 112, article 110787, 2021.

[11] Z. Wang, L. Zhang, Y. Hao et al., "Ratiometric fluorescent sensors for sequential on-off-on determination of riboflavin, Ag^{+} and l-cysteine based on NPCl-doped carbon quantum dots," *Analytica Chimica Acta*, vol. 1144, pp. 1–13, 2021.

[12] C. Lu, D. Chen, Y. Duan et al., "New properties of carbon nanomaterials through zinc doping and application as ∗∗ a∗∗ ratiometric fluorescence pH sensor," *Materials Research Bulletin*, vol. 142, article 111410, 2021.

[13] C. Wang, H. Shi, M. Yang et al., "Biocompatible sulfur nitrogen co-doped carbon quantum dots for highly sensitive and selective detection of dopamine," *Colloids and Surfaces. B, Biointerfaces*, vol. 205, article 111874, 2021.

[14] X. Kou, S. Jiang, S.-J. Park, and L.-Y. Meng, "A review: recent advances in preparations and applications of heteroatom-doped carbon quantum dots," *Dalton Transactions*, vol. 49, no. 21, pp. 6915–6938, 2020.

[15] S. Kaushal, M. Kaur, N. Kaur, V. Kumari, and P. P. Singh, "Heteroatom-doped graphene as sensing materials: a mini review," *RSC Advances*, vol. 10, no. 48, pp. 28608–28629, 2020.

[16] S. Chandra, A. R. Chowdhuri, D. Laha, and S. K. Sahu, "Fabrication of nitrogen- and phosphorous-doped carbon dots by the pyrolysis method for iodide and iron(III) sensing," *Luminescence*, vol. 33, no. 2, pp. 336–344, 2018.

[17] J. Chen, J. Shu, J. Chen, Z. Cao, A. Xiao, and Z. Yan, "Highly luminescent S,N co-doped carbon quantum dots-sensitized chemiluminescence on luminol-H2O2system for the determination of ranitidine," *Luminescence*, vol. 32, no. 3, pp. 277–284, 2017.

[18] N. Li, F. Lei, D. Xu, Y. Li, J. Liu, and Y. Shi, "One-step synthesis of N, P co-doped orange carbon quantum dots with novel optical properties for bio-imaging," *Optical Materials*, vol. 111, article 110618, 2021.

[19] X. Ma, S. Li, V. Hessel, L. Lin, S. Meskers, and F. Gallucci, "Synthesis of N-doped carbon dots via a microplasma process," *Chemical Engineering Science*, vol. 220, article 115648, 2020.

[20] L. Ansari, S. Hallaj, T. Hallaj, and M. Amjadi, "Doped-carbon dots: recent advances in their biosensing, bioimaging and therapy applications," *Colloids and Surfaces. B, Biointerfaces*, vol. 203, article 111743, 2021.

[21] R. Wang, K.-Q. Lu, Z.-R. Tang, and Y.-J. Xu, "Recent progress in carbon quantum dots: synthesis, properties and applications in photocatalysis," *Journal of Materials Chemistry A*, vol. 5, no. 8, pp. 3717–3734, 2017.

[22] D. Kumar, K. Singh, V. Verma, and H. S. Bhatti, "Synthesis and characterization of carbon quantum dots from orange juice," *Journal of Bionanoscience*, vol. 8, no. 4, pp. 274–279, 2014.

[23] J. Xu, T. Lai, Z. Feng, X. Weng, and C. Huang, "Formation of fluorescent carbon nanodots from kitchen wastes and their

application for detection of Fe3+," *Luminescence*, vol. 30, no. 4, pp. 420–424, 2015.

[24] S. Miao, K. Liang, J. Zhu, B. Yang, D. Zhao, and B. Kong, "Hetero-atom-doped carbon dots: doping strategies, properties and applications," *Nano Today*, vol. 33, article 100879, 2020.

[25] Z. Zhang, G. Yi, P. Li et al., "A minireview on doped carbon dots for photocatalytic and electrocatalytic applications," *Nanoscale*, vol. 12, no. 26, pp. 13899–13906, 2020.

[26] L. Đorđević, F. Arcudi, and M. Prato, "Preparation, functionalization and characterization of engineered carbon nanodots," *Nature Protocols*, vol. 14, no. 10, pp. 2931–2953, 2019.

[27] G. Cairo and A. Pietrangelo, "Iron regulatory proteins in pathobiology," *The Biochemical Journal*, vol. 352, no. 2, pp. 241–250, 2000.

[28] M. W. Hentze, M. U. Muckenthaler, B. Galy, and C. Camaschella, "Two to tango: regulation of mammalian iron metabolism," *Cell*, vol. 142, no. 1, pp. 24–38, 2010.

[29] G. Papanikolaou and K. Pantopoulos, "Iron metabolism and toxicity," *Toxicology and Applied Pharmacology*, vol. 202, no. 2, pp. 199–211, 2005.

[30] P. Aisen, M. Wessling-Resnick, and E. A. Leibold, "Iron metabolism," *Current Opinion in Chemical Biology*, vol. 3, no. 2, pp. 200–206, 1999.

[31] D. Gomes, M. Segundo, J. Lima, and A. Rangel, "Spectrophotometric determination of iron and boron in soil extracts using a multi-syringe flow injection system," *Talanta*, vol. 66, no. 3, pp. 703–711, 2005.

[32] C. M. G. van den Berg, "Chemical speciation of iron in seawater by cathodic stripping voltammetry with dihydroxynaphthalene," *Analytical Chemistry*, vol. 78, no. 1, pp. 156–163, 2006.

[33] E. Li, J. Kang, P. Ye, W. Zhang, F. Cheng, and C. Yin, "A prospective material for the highly selective extraction of lithium ions based on a photochromic crowned spirobenzopyran," *Journal of Materials Chemistry B*, vol. 7, no. 6, pp. 903–907, 2019.

[34] R. Wang, L. Diao, Q. Ren, G. Liu, and S. Pu, "New bifunctional diarylethene sensor for multianalyte detection and Al3+ imaging in live cells," *ACS Omega*, vol. 4, no. 1, pp. 309–319, 2019.

[35] A. Kumar, P. R. Sahoo, P. Arora, and S. Kumar, "A light controlled, sensitive, selective and portable spiropyran based receptor for mercury ions in aqueous solution," *Journal of Photochemistry and Photobiology A: Chemistry*, vol. 384, article 112061, 2019.

[36] D. A. Gupta, M. L. Desai, N. I. Malek, and S. K. Kailasa, "Fluorescence detection of Fe^{3+} ion using ultra-small fluorescent carbon dots derived from pineapple (Ananas comosus): Development of miniaturized analytical method," *Journal of Molecular Structure*, vol. 1216, article 128343, 2020.

[37] M. L. Desai, H. Basu, S. Saha, R. K. Singhal, and S. K. Kailasa, "Investigation of silicon doping into carbon dots for improved fluorescence properties for selective detection of Fe^{3+} ion," *Optical Materials*, vol. 96, article 109374, 2019.

[38] S. K. Tammina, Y. Wan, Y. Li, and Y. Yang, "Synthesis of N, Zn-doped carbon dots for the detection of Fe^{3+} ions and bactericidal activity against Escherichia coli and Staphylococcus aureus_," *Journal of Photochemistry and Photobiology. B*, vol. 202, article 111734, 2020.

[39] Y. Kang, Y. Yang, L.-C. Yin, X. Kang, G. Liu, and H.-M. Cheng, "An amorphous carbon nitride photocatalyst with greatly extended visible-light-responsive range for photocatalytic hydrogen generation," *Advanced Materials*, vol. 27, no. 31, pp. 4572–4577, 2015.

[40] X. Gong, W. Lu, M. C. Paau et al., "Facile synthesis of nitrogen-doped carbon dots for Fe^{3+} sensing and cellular imaging," *Analytica Chimica Acta*, vol. 861, pp. 74–84, 2015.

[41] G. Dong, K. Lang, H. Ouyang et al., "Facile synthesis of N, P-doped carbon dots from maize starchviaa solvothermal approach for the highly sensitive detection of Fe3+," *RSC Advances*, vol. 10, no. 55, pp. 33483–33489, 2020.

[42] Z. Yi, X. Li, H. Zhang et al., "High quantum yield photoluminescent N-doped carbon dots for switch sensing and imaging," *Talanta*, vol. 222, p. 121663, 2021.